Protons in Non-ionic Aqueous Reverse Micelles

Javier Rodriguez,[†,‡] Jordi Martí,[§] Elvira Guàrdia,[§] and Daniel Laria*[,†,‡]

Departamento de Química Inorgánica, Analítica y Qumica-Física e INQUIMAE, Facultad de Ciencias Exactas y Naturales, Universidad de Buenos Aires, Ciudad Universitaria, Pabellón II, 1428, Buenos Aires, Argentina, Unidad Actividad Física, Comisión Nacional de Energía Atómica, Avenida Libertador 8250, 1429, Buenos Aires, Argentina, and Departament de Física i Enginyeria Nuclear, Universitat Polytècnica de Catalunya, B4-B5 Campus Nord, 08034 Barcelona, Spain

Received: January 15, 2007; In Final Form: February 28, 2007

Using molecular dynamics techniques, we investigate the solvation of an excess proton within an aqueous reverse micelle in vacuo, with the neutral surfactant diethylene glycol monodecyl ether [$CH_3(CH_2)_{11}(OC_2H_4)_2$-OH]. The simulation experiments were performed using a multistate empirical valence bond Hamiltonian model. Our results show that the stable solvation environments for the excess proton are located in the water−surfactant interface and that its first solvation shell is composed exclusively by water molecules. The relative prevalence of Eigen- versus Zundel-like solvation structures is investigated; compared to bulk results, Zundel-like structures in micelles become somewhat more stable. Characteristic times for the proton translocation jumps have been computed using population relaxation time correlation functions. The micellar rate for proton transfer is approximately 40× smaller than that found in bulk water at ambient conditions. Differences in the computed rates are examined in terms of the hydrogen-bond connectivity involving the first solvation shell of the excess charge with the rest of the micellar environment. Simulation results would indicate that proton transfers are correlated with rare episodes during which the HB connectivity between the first and second solvation shells suffers profound modifications.

I. Introduction

Reverse micelles are amphiphilic structures spontaneously generated when surfactants are mixed with nonpolar solvents. The addition of small amounts of a third polar component normally leads to the formation of confined pools surrounded by surfactant headgroups. As such, these liquid phases exhibit structural and dynamical properties well differentiated from what is normally perceived in more conventional, i.e., bulk-like phases.[1−3] These "unusual" properties derive from the nature of the prevailing confinement, which plays a key role in regulating chemical reactivity within these supramolecular assemblies. In most cases, the characteristics of the confinement can be conveniently gauged by controlling the chemical properties of the surfactant species and w_o, the relative concentrations of polar and surfactant components as well.

From a microscopic perspective, the gross structural characteristics of polar phases within reverse micelles are usually portrayed in terms of roughly spherical domains in which it is possible to distinguish different regions: (i) On one hand, there is an external shell, lying in close contact with the surfactant groups (and eventually counterions, in the presence of ionic surfactants). Molecules residing in this outer shell exhibit important modifications in their intermolecular connectivity and in their dynamical modes; most notable are those related to the drastic retardations operated in translational and rotational motions.[4,5] (ii) On the other hand, there is a central region, where effects from confinement are less severe, leading to somewhat milder modifications in the structure and the dynamics. Of course, the prevalence and proper identification of these regions depend on the micellar size considered.[6] Moreover, in some cases, this two-region description may even become inappropriate: For instance, it is normally accepted that, for $w_o \lesssim 5$, practically all water molecules confined in aqueous reverse micelles are bound to the interface (i.e., absence of central region).[7] From the previous considerations, these confined liquid-like phases could be pictured as nanodomains, in which spatial inhomogeneities prevail over length scales comparable to their overall sizes.

The present paper deals with reactivity of protons in aqueous reverse micelles; more specifically, we analyze the solvation of an excess positive charge dissolved in a water pool, surrounded by neutral surfactants. It would be redundant to emphasize here the importance of protons as fundamental ionic species regulating chemical reactivity in all aqueous environments. For the specific case of reverse micelles, there is a large body of previous studies[8−13] that have analyzed the role of the predominant pH as a controlling agent in acid−base equilibria, catalysis processes, hydrolysis, etc. At present, there seems to be sufficient experimental evidence indicating that the presence of surfactants and/or counterions induce important fluctuations in the local concentrations of protons within aqueous reverse micelles. For example, Hasegawa has reported that water pools in AOT (aerosol sodium bis-(2-ethylhexyl)sulfosuccinate) reverse micelles present buffer-like characteristics.[8] Using pyranine as a pH probe, Hasegawa found practically no changes in the probe excitation spectra—corresponding to a local intramicellar pH of ∼5—regardless of the adjusted pH of the bulk solution before solubilization (intermediate between 3 and 11). More recently, NMR experiments by Baruah et al.[10] indicate increasing proton concentrations within reverse micelles as one

* Corresponding author. E-mail: dhlaria@cnea.gov.ar.
† Departamento de Química Inorgánica.
‡ Unidad Actividad Física.
§ Departament de Física i Enginyeria Nuclear.

10.1021/jp0703410 CCC: $37.00 © 2007 American Chemical Society
Published on Web 04/11/2007

moves from a neutral central nucleus toward more acidic interfacial regions.

Aqueous protons also play a fundamental role, controlling proton-transfer reactions involving the solvent within reverse micelles. Bardez et al.[11] and Politi et al.[12] have examined excited-state proton-transfer reactions of different fluorescent probes and have compared the observed rates to those observed in bulk water. One important finding reported in these works is the clear correlation that exists between changes in the observed rates and modifications in the local solvation structures. Similar conclusions pertaining to the reactivity−structure relationship have been obtained by Cohen et al.[13] in their study of the complex process involving the proton release from 2-naphtol-6,8-disulfonate into the water nanopool.

The analyses presented in this paper rely on the use of molecular dynamics simulation experiments. This approach has been implemented in the past to examine a large variety of reverse micellar environments, with different degrees of molecular detail in the modeling of the polar and nonpolar phases and the surfactant groups as well.[14−24] For the particular case of non-ionic reverse micelles, two previous simulation studies are worth commenting: Allen et al.[24] have examined the structural and dynamical aspects of a model $w_o \sim 2.5$ micelles with diethylene glycol monodecyl ether ($C_{12}E_2$) as a surfactant. More recently, Abel et al.[22] have modeled aqueous reverse micelles ($w_o = 3$) with a longer surfactant ($C_{12}E_4$) and have analyzed effects from conformational equilibria in the surfactants on the dynamical modes of the trapped water. In the present case, we followed closely the model proposed by Allen et al.[24] Their results show that, when solubilized in bulk decane, the interior of the micelle looks like a distorted, spherical-like structure with an average radius intermediate between 7 and 10 Å. More interestingly, Allen et al. have reported that the main structural characteristics of the inner water pool and the surfactant groups in close contact with the aqueous phase remained practically unchanged when the nonpolar phase was removed (i.e., micelle in vacuum). These characteristics have been recently exploited in a series of recent papers by Faeder and Ladanyi, who modeled aqueous reverse micelles without the explicit incorporation of the nonpolar phase.[14−16]

To describe the excess proton, we adopted a methodology based on a multi-state empirical valence bond (MS-EVB) model Hamiltonian. The implementation of this approach to the analysis of chemical reactivity in condensed media has been pioneered by Warshel and collaborators.[25] For aqueous protons, MS-EVB schemes have been successfully adapted to analyze solvation at ambient conditions,[27−39] supercritical states,[40] mixtures,[41] and confined environments as well.[42−44] Two features of this methodology are worth comment: (i) it provides a quite accurate parametrization of the force field acting on the proton at reasonable computer costs, and (ii) it incorporates the mechanism of proton translocation—a key aspect in proton-transfer processes in water—in a natural fashion. With this implementation, not only did we succeed in analyzing equilibrium aspects pertaining to the proton solvation structures within the micelles but we have also examined dynamical aspects related to the rates of proton transfers and possible mechanisms that trigger proton jumps between neighboring water molecules.

The organization of the present work is as follows: In the next section, we present an overview of the model and the simulation procedure. The central part of the paper (Section III) is devoted to the simulation results and includes a description of the solvation structures of the excess proton in reverse micelles. In Section IV, dynamical aspects of proton transfer are presented. The concluding remarks are summarized in the last section.

II. Model and Simulation Procedure

To undertake the molecular dynamics experiments, we adopted an MS-EVB model. Details of this model have been extensively described in previous publications, so we will briefly comment here on its main features and refer the interested reader to refs 26−31 for more comprehensive presentations.

The key element of the model is the following MS-EVB Hamiltonian:

$$\hat{H}_{EVB}(\{\mathbf{R}\}) = \sum_{ij} |\phi_i\rangle h_{ij}(\{\mathbf{R}\})\langle\phi_j| \quad (1)$$

where $\{|\phi_i\rangle\}$ represents a basis set of diabatic states, each one denoting spatial localization of the excess proton in the tagged i-th water molecule. The different matrix elements $h_{ij}(\{\mathbf{R}\})$ are functions of the nuclear coordinates and are adjusted so that the geometry and the energy of small protonated water clusters obtained from the ground state of the Hamiltonian present good agreement with highly sophisticated quantum mechanical ab initio calculations.[29] At each step of the simulation, the instantaneous diabatic states are determined by establishing a connectivity pattern of hydrogen bonds (HB) started at the position of the excess charge (hereafter referred to as the pivot water and denoted H_2O^*). Details of this procedure can be found in refs 29−34. Typically, the number of diabatic states included in the construction of $\hat{H}_{EVB}$ was ∼10.

The dynamics of the nuclei of mass M_k are obtained from $\epsilon_0(\{\mathbf{R}\})$, the instantaneous lowest eigenvalue of $\hat{H}_{EVB}$, namely

$$M_k \frac{d^2\mathbf{R}_k}{dt^2} = -\nabla_{\mathbf{R}_k}\epsilon_0(\{\mathbf{R}\}) \quad (2)$$

In the previous equation, $\epsilon_0(\{\mathbf{R}\})$ satisfies

$$\hat{\mathbf{H}}_{EVB}|\psi_0\rangle = \epsilon_0(\{\mathbf{R}\})|\psi_0\rangle \quad (3)$$

where $|\psi_0\rangle$ is the instantaneous MS-EVB ground state. Expressed in terms of the diabiatic basis, $|\psi_0\rangle$ can be written as

$$|\psi_0\rangle = \sum_i c_i|\phi_i\rangle \quad (4)$$

Using eqs 1, 3 and 4, we can rewrite the equations of motion as

$$M_k \frac{d^2\mathbf{R}_k}{dt^2} = -\sum_{i,j} c_i c_j \nabla_{R_k} h_{ij}(\{\mathbf{R}\}) \quad (5)$$

At each time step of the simulation, the index of the largest expansion coefficient, c_i, determines the water molecule that exhibits stronger H_3O^+ character, which can eventually be updated, in the event of a proton translocation episode.

Diagonal elements $h_{ii}(\{\mathbf{R}\})$ include inter- and intramolecular interactions involving the tagged H_3O^+ group and the rest of the water molecules,[29] that were modeled using the flexible TIP3 model.[45] In addition, these interactions were supplemented with contributions involving the surfactant sites.

Using the united atom limit for the CH_3 and CH_2 groups, we found that $C_{12}E_2$ molecules $[CH_3(CH_2)_{11}(OC_2H_4)_2OH]$ comprised a total of 20 interactions sites. Intramolecular interactions in the surfactant molecules included stretching, bending, non-

bonding, and dihedral modes; energy, length, and charge parameters for these interactions were taken from ref 44. No changes were operated in the functionality of the non-diagonal coupling elements from what has been reported in ref 29.

The eventual inclusion of diabatic states localized in oxygen sites of the surfactant (hydroxyl and/or ether groups) was not contemplated in this study. We adopted this approximation after analyzing the acidic characteristics of several compounds of the type $[R-OH_2]^+$ ($pK_a \sim -2.2$) and $[R-OH-R']^+$ ($pK_a \sim -3.8$); clearly, the latter moieties behave as stronger acids than H_3O^+ ($pK_a \sim -1.7$). Anyhow, the real importance of the explicit inclusion of such species in the description of the proton solvation seems to be under debate. On the basis of experimental evidence,[47] a recent EVB study of methanol−water mixtures[41] suggests that, compared to H_3O^+, the presence of protonated methanol could be safely disregarded. On the other hand, this assumption seems to clash with ab initio simulation results for similar mixtures,[48] which show non-negligible branching ratios for equilibria of the type

$$H_3O^+ + MeOH \rightleftharpoons H_2O + MeOH_2^+ \qquad (6)$$

As such, the issue still awaits proper clarification.

To build $C_{12}E_2$ reverse micelles in vacuo, we followed closely the procedure proposed by Allen et al.[24] Briefly, a spherical sample of radius ~9.5 Å, containing $N_w = 119$ water molecules, was extracted from an equilibrated bulk system at $T = 298$ K. In addition, a total of $N_s = 50$ surfactant molecules were evenly distributed at the vicinity of the free interface of the water sample (this yields $w_o = 2.4$). The initial intramolecular configurations of the hydrophobic tails corresponded to fully trans conformers; their head-to-tail vectors were oriented pointing radially outward. The system was then equilibrated for about 300 ps, allowing the surfactant headgroups to get in contact with the water substrate. A subsequent equilibration period of ~250 ps followed, during which only the tail groups were allowed to move at a temperature close to 700 K. From then on, the system was gradually cooled down to temperatures close to 20 K during ~250 ps; ambient conditions were slowly recovered during a subsequent time interval of ~250 ps. The last procedure involved the replacement of a central water molecule by a hydronium molecule, followed by a final 200 ps equilibration period, during which all particle velocities were rescaled (with values corresponding to $T = 298$ K) at 5 ps time intervals. Meaningful statistics were harvested along 5 ns microcanonical trajectories.

III. Micellar Solvation of H^+

Before addressing the analysis of protonic states in aqueous reverse micelles, it will be instructive to briefly review a few important aspects pertaining to the structural characteristics of these confined environments, which, in turn, may predetermine the resulting solvation of the excess charge. Some of these features have already been reported elsewhere.[24]

The micelle represents an inhomogeneous environment, so our description will be facilitated by the consideration of a reference frame, with the origin located at the center of mass of the aggregate. In Figure 1, we show results for local densities of different species as a function of the distance r measured from the center of the micelle. More specifically, the curves represent results for

$$\rho_{CM-\alpha}(r) = \frac{1}{4\pi r^2}\left\langle \sum_i \delta(|r_i^\alpha - R_{CM}| - r)\right\rangle \qquad (7)$$

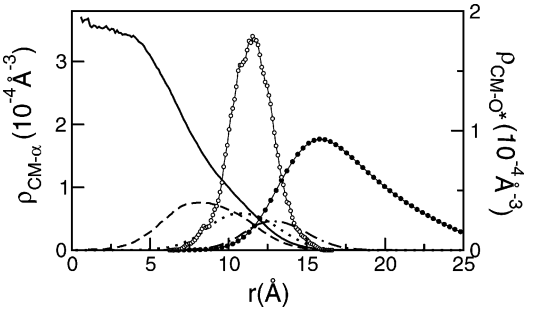

Figure 1. Density fields for different species in the aqueous reverse micelles: water (solid line), hydroxyl groups (dashed line), ether-oxygens (dotted and dash-dotted lines), methyl and methylene groups (black circles). The proton location is characterized by the distribution for the pivot O* (open circles, right axis).

where r_i^α denotes the coordinate of the site α in the i-th molecule and R_{CM} represents the coordinate of the center of mass of the micelle. The profiles for the oxygen sites in water and for the surfactant sites (in Figure 1, we discriminate results for the distal hydroxyl, the two ether-oxygen groups, and all carbon sites in the hydrophobic tails) look similar to those previously reported by Allen et al.[24] and agree, at a qualitative level, with results from simulations in which the nonpolar phase was explicitly incorporated.

In particular, note that although the central nucleus of water presents a density close to the standard bulk value for water at ambient conditions, $\rho_w \sim 3 \times 10^{-2}$ Å^{-3}, at the micelle boundary, the density presents a smooth decay over a fairly wide interval, $5 \lesssim r \lesssim 15$ Å. This interval is comparable to the original radius of the water sample. The characteristics of this decay reflect two different features of the water pool: (i) the anisotropy of its overall shape and (ii) the roughness of the water/surfactant interface characterized by the presence of a series of protruding clustered structures, comprising 3−5 molecules. These clusters are localized in cavities within spatial domains of the surfactants headgroups and usually present low—and even temporary absence of—HB connectivity with the rest of the inner water phase. Moreover, in the course of a fairly long trajectory, these clusters undergo modifications in shape and in size, becoming eventually incorporated into the central water core and/or reappearing in the form of new structures, in different locations of the water/surfactant interface. These fluctuations involving a global reorganization of the water boundary are normally slow processes, characterized by time scales intermediate between tens and a few hundreds of picoseconds. In panel A of Figure 2, we show a snapshot of a typical micellar configuration, where a few of these external clustered structures are clearly perceptible.

Focusing now on the specific solvation of the proton, a preliminary consideration is in order. We mentioned in the previous section that, at the beginning of the simulation runs, the excess charge was inserted at the center of the aggregate and allowed to freely explore different micellar environments. In all cases investigated, we found that after a few tens of picoseconds, the excess charge migrates toward the boundary of the water pool and gets trapped normally within one of the above-mentioned external water pockets. Note that the density profile for the proton shown in Figure 1 is accordant with this observation because the overall distribution is centered at $r \sim 11.9$ Å.

Concerning the closest solvation environment of the excess charge, there seems to be general consensus that the microscopic

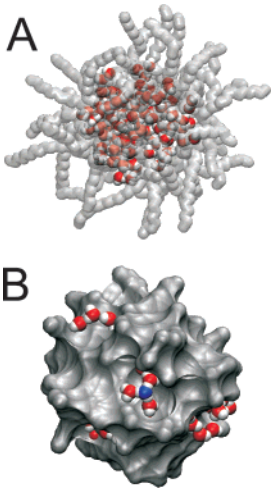

Figure 2. (A) Snapshot of a configuration for a $C_{12}E_2$ reverse micelles ($w_o \sim 2.5$). For clarity purposes, the surfactants appear in shaded colors. (B) Snapshot of a typical solvation environment for an excess proton in a $C_{12}E_2$ reverse micelles. Only hydroxyl groups (dark gray) are shown in surfactants; the pivot oxygen is rendered in blue.

description of H^+ in bulk water includes a whole series of structures that are intermediate between the following two moieties: the symmetric Zundel (ZDL) dimer[49] $[H_2O-H-OH_2]^+$ and the so-called Eigen (EGN) cation[50] $[H_3O\cdot(H_2O)_3]^+$. In bulk water at ambient conditions, interconversions between these limiting structures take place in the picosecond time scale and are operated via subtle modifications in the intermolecular distances and in the connectivity pattern involving the proton closest solvation shells. As we will show in what follows, the spatial confinement prevailing within the micelle modifies the previous description in a sensible fashion.

The implementation of an MS-EVB approach provides an appropriate order parameter ξ to monitor EGN−ZDL interconversions; expressed in terms of the two largest expansion coefficients (c_1 and c_2), ξ can be written as[29,31]

$$\xi = c_1^2 - c_2^2 \tag{8}$$

Note that the limiting EGN and ZDL solvation environments are characterized by values of ξ close to 1 and 0, respectively. In this context, it will be useful to analyze the free energy, $W(\xi)$, associated with the order parameter, namely

$$\beta W(\tilde{\xi}) \propto -\ln\langle\delta(\xi - \tilde{\xi})\rangle \tag{9}$$

where β is the inverse of Boltzmann constant times the temperature and $\langle ... \rangle$ represents a statistical average.

Results for $W(\xi)$ are depicted in Figure 3, where we have also included results for bulk water at ambient conditions taken from refs 29 and 31. We remark that the most stable structures in micelles, which correspond to the global minimum of $W(\xi)$, are characterized by values of ξ_{min} somewhat smaller than those for the case of bulk water (0.45 versus 0.55), suggesting a larger extent of proton delocalization (expressed in terms of a more marked tendency toward resonant ZDL configurations) in micellar states. Moreover, also note that the magnitude of the overall free energy difference between EGN- and ZDL-like structures also decreases; as a consequence, in the course of a trajectory, episodes during which the proton resonates between two tagged water molecules are likely to be found more often.

Quantitative estimates of the relative prevalence of these limiting structures can be extracted from an equilibrium constant,

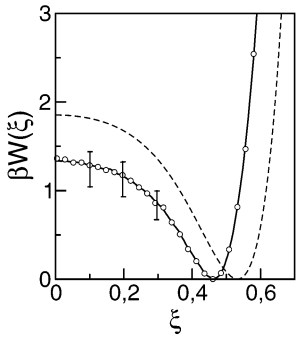

Figure 3. Free energy associated to the asymmetric order parameter ξ describing Eigen−Zundel interconversions in reverse micelles (open circles). Also shown are results for bulk water (dashed line) extracted from refs 28 and 30. The curves were brought to the same reference value at their corresponding minima.

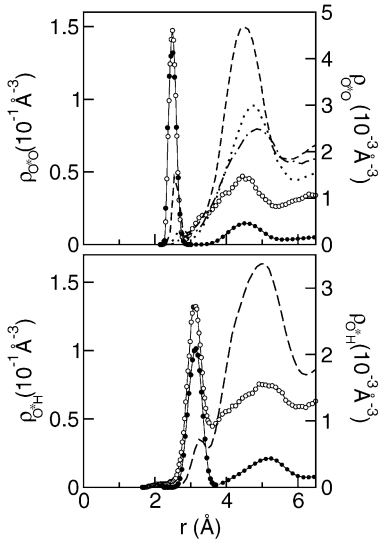

Figure 4. Top panel: Oxygen pivot-solvent oxygen site pair correlations in aqueous reverse micelles: water-oxygen (black circles, left axis), hydroxyl surfactant (dashed line, right axis), ethoxy 1 surfactant (dotted line, right axis), ethoxy 2 surfactant (dot-dashed line, right axis). Also shown are results for water-oxygen in bulk water (open circles, left axis) (ref 28). Bottom panel: oxygen pivot-hydrogen solvent pair correlations in aqueous reverse micelles. The labeling is the same as the one used in the top panel.

K_{eq}, defined in terms of equilibrium concentrations x_i (i = EGN, ZDL), namely[51]

$$K_{eq} = \frac{x_{EGN}}{x_{ZDL}} \sim e^{-\beta[W(\xi=\xi_{min})-W(\xi=0)]} \tag{10}$$

K_{eq} was found to be ~3.9 and 6.7 for micelles and bulk environments, respectively.

The local coordination of the excess charge was analyzed by computing pair correlations involving the O* site. In the top panel of Figure 4, we show plots for pair correlations involving the pivot O* and the rest of water-oxygen sites; also shown are plots describing spatial correlations with respect to hydroxyl- and ether-oxygens in the surfactants. Correlations with the aqueous phase are dominated by a main peak located at $r \sim 2.5$ Å (black circles); its area includes ~ 2.9 water-oxygen sites acting as HB acceptors. Note that the magnitude and the position of this peak are similar to the ones observed in bulk water[29] (shown in open circles), suggesting that the three-donor coordination that distinguishes the solvation of the H_3O^+ cation in bulk is preserved in the micellar environment. The magnitude

of the closest peak for the oxygen site of the distal hydroxyl in the headgroups—shifted 0.1 Å outward—is 2 orders of magnitude smaller than the one observed for water, revealing that oxygen sites in the surfactant molecules very rarely act as potential HB acceptors from the hydronium. On the other hand, note that the curves for the latter sites show broad peaks located at ~3.8 Å, which gradually decrease in magnitude as we move from the distal OH toward the two ether-oxygens. The locations of these peaks roughly coincide with the one for the second water-oxygen peak, indicating that surfactant sites would participate in the second and, eventually, more external solvation shells of the excess proton.

The absence of coordination of the type OH···O* is confirmed by the plots shown in the bottom panel. Note that the first peak is shifted approximately 1.1 Å away from the position of the curves shown in the top panel and that its area includes roughly the six hydrogen atoms belonging to water molecules lying in the first solvation shell. Given this evidence, and should this picture remain valid in the case of considering the explicit presence of the nonpolar phase, the characteristics of the closest environment of the hydronium cation in these neutral micelles could be summarized as follows: (i) localization of the excess charge in external water pockets located within spatial domains of the surfactants and exhibiting low HB connectivity with the rest of the water sample; (ii) persistence of three-coordination, exclusively with water molecules in the substrate, which act as HB acceptors; (iii) polar surfactant sites participating in the second or outer solvation shells of H_3O^+. These three distinctive features are clearly illustrated in panel B of Figure 2. As we will see in the next section, these characteristics will have important implications determining rates and possible mechanisms for proton transfer in micelles.

IV. Proton Transfer

Having established the main features of the equilibrium solvation structures, we now move to the consideration of the dynamical characteristics related to proton-transfer processes in micelles. Rates for proton transfer can be extracted from population relaxation time correlation functions of the type

$$C(t) = \frac{\langle \delta h_i(t) \cdot \delta h_i(0) \rangle}{\langle (\delta h_i)^2 \rangle} \tag{11}$$

where $\delta h_i(t) = h_i(t) - \langle h_i \rangle$ denotes the instantaneous fluctuation of the population of the *i*-th reactant away from its equilibrium value. In eq 11, the dynamical variable $h_i(t)$ is unity if the proton is localized in the *i*-th diabatic state at time *t* and zero otherwise. Should Onsager's regression hypothesis[52] remain valid, the exponential decay at long times of $C(t)$ should yield an estimate of the proton-transfer rate, τ_{tr}^{-1}.

A plot of $C(t)$ obtained from an average of five statistically independent trajectories, each one lasting 5 ns, is presented in Figure 5; in the inset of the figure, we have also included results for a similar decay of $C(t)$ for bulk water. The large disparity between the scales in the temporal axes reflects the dramatic changes in the rates of proton transfer; note that the micelle characteristic time for translocations, $\tau_{tr}^{mic} \sim 130$ ps, is more than 1 order of magnitude larger than the results for bulk water at ambient conditions, $\tau_{tr}^{bulk} \sim 4$ ps.

Given the sharp distinctions between the proton solvation structures in micellar and bulk environments, the modifications operated in the characteristic time scales are not totally unexpected. As possible reasons to account for these differences, one could in the first place invoke the global retardation of the diffusive and rotational motions experienced by water molecules confined in reverse micelles.[15] Moreover, it is also well-established that the overall slowness of the aqueous phase is not uniform, being more marked in micellar environments located in the close vicinity of the surfactant groups. These environments, in turn, correspond to regions likely to host the excess charge; so, the observed alterations in the dynamics of the proton closest solvation shells will necessarily affect the transfer rates.

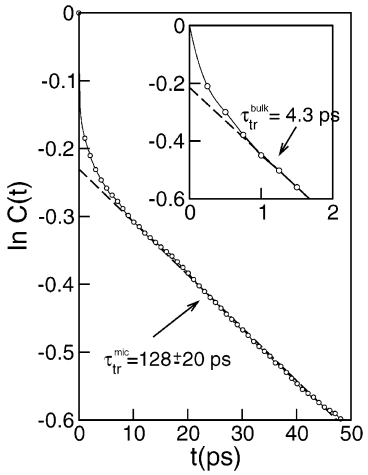

Figure 5. Logarithm of the population relaxation of the pivot label in reverse micelles. The inset shows similar results for bulk water at ambient conditions taken from ref 30.

The characterization of the microscopic mechanisms that trigger proton transfers in aqueous media has received considerable attention in recent years.[53] Although the subject still presents some controversial issues, there seems to be sufficient indications suggesting that the time limiting steps are to be found in modifications in the connectivity pattern involving the first, second—and perhaps even outer—solvation shells. Guided by this evidence and looking for clues that would allow us to rationalize the large differences observed in the characteristic time scales, we examined in detail the HB connectivity between the first solvation shell and the rest of the micelle.

It will be convenient to begin our analysis by considering as a reference benchmark the results depicted in the top panel of Figure 6. The plots correspond to spatial correlations between surfactants and nearby water molecules in the central pool. The curves look similar to those presented in Figure 6 of ref 24 and clearly reflect two features: (i) first, the HB donor character of the distal hydroxyl group in the surfactant, indicated by the main peaks located at $r = 1.8$ and 2.9 Å; (ii) second, the two curves involving the two ether-oxygens (O_1 and O_2), which are consistent with a water-bridged structure of HB of the type $O_1 \cdot\cdot\cdot H_w \cdot\cdot\cdot O_2$.[54]

The coordination involving surfactants and water molecules lying in the proton first solvation shell is shown in the middle panel and contrasts sharply with the previous description. First, note that the first main peak has disappeared, revealing that these water molecules receive no HB from the distal hydroxyl groups. Moreover, the plots and the magnitude of the cumulative integrals shown in the right-hand side axis would indicate that they donate one HB equally likely to either a distal hydroxyl group or to the two ether-oxygens (via the bridged HB structure mentioned above). The data shown in the bottom panel complete the description and correspond to correlations involving the rest of the aqueous phase. The main peaks located at $r = 1.8$ and 2.8 Å are the dominant features of ρ_{HO} and ρ_{OO}, respectively, and each one involves approximately one site in the rest of the

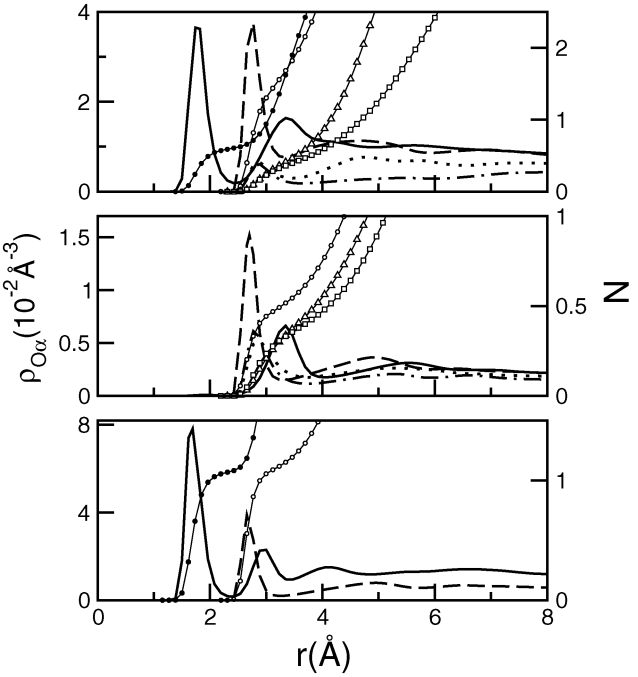

Figure 6. Top panel: pair correlation functions involving surfactant sites and water-oxygens in aqueous reverse micelles (left axis); also shown are results for cumulative integrals (symbols, right axis). H (hydroxyl group): solid line and black circles. O (hydroxyl group): dashed line and open circles. Ethoxy-ether 1: dotted line and triangles. Ethoxy-ether 2: dot-dashed and diamonds. Middle panel: correlations involving surfactant sites and water-oxygen in the first solvation shell of the proton (same labeling as in the top panel). Bottom panel: correlations involving the water in the proton first solvation shell and the rest of water-oxygens. H−O: solid line, black circles. O−O: dashed line, open circles (same labeling as in the top panel).

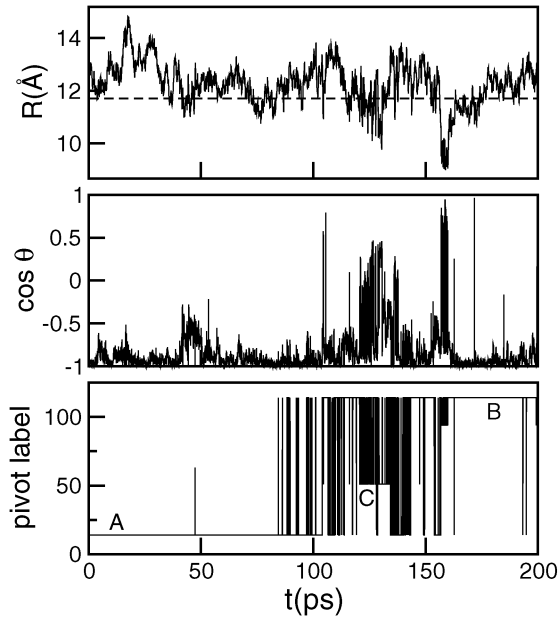

Figure 7. Time evolutions of different pivot observables during a proton transfer. Top panel: distance to the micelle center. Central panel: dipolar alignment of H_3O^+. Bottom panel: pivot label (see text). The dashed line in the top panel corresponds to the average micellar radius.

aqueous phase. The overall picture that emerges from all these considerations can be summarized as follows: Compared to what is observed in water molecules lying in the close vicinity of the surfactant groups, the presence of an excess proton modifies the connectivity pattern between water molecules lying at its first solvation shell and the rest of the micelle. These "special" molecules receive only one HB from the H_3O^+ and act as double HB donors. Usually, one of these HB involves an oxygen site in the surfactants, and the other is shared with a second acceptor water lying in an outer shell.

In this context, a pertinent question to be raised concerns whether the solvation characteristics described above can explain the observed retardation in the mechanisms that drive proton transfer in micelles. Before affording a plausible explanation, it will be useful to complement the previous analysis with a closer look into the temporal behavior of a series of relevant observables during one particular proton-transfer event; this episode bears common characteristics with many other encountered in the course of our simulation experiments.

In the bottom panel of Figure 7, we display results for the evolution of the pivot label: The trajectory presents three, well differentiated, temporal domains: (i) During the first ~80 ps, the system remains in the reactant side, as the proton is localized in the single pivot water molecule labeled *A*. (ii) The subsequent 50 ps period is an intermediate stage, characterized by Zundel-like resonances between the original pivot *A* and a nearest water neighbor *B*. Note that the trajectory also includes a brief episode (120 ps $\lesssim t \lesssim$ 130 ps), during which the resonance involves a third water molecule *C*. (iii) After $t \sim 150$ ps, the transfer process is completed, and the proton gets localized in state *B*.

The middle panel includes results for cos θ, i.e., the projection of the dipole moment of the instantaneous pivot H_3O^+ along the direction of the micelle radius. Note that stable reactant and product states, *A* and *B*, clearly correlate with dipolar orientations along the radius of the micelle and pointing inward. On the other hand, during the resonance episodes, the orientation of the dipole moment presents abrupt changes, remaining even perpendicular to its original orientation. A simple geometrical construction is sufficient to reveal that this arrangement is accordant with a ZDL complex, with its O···H···O symmetry axis oriented along the radius of the aggregate.

In the top panel of Figure 7, we monitor the distance $R(t) = |r_{O^*}(t) - R_{CM}|$. At a first glance, the temporal dependence of this variable presents fast fluctuations in the subpicosecond time domain that modulate a much slower dynamical mode involving characteristic times of the order of a few tens of picoseconds. Perhaps even more interesting is to verify that the persistence of resonances—and more importantly, the final stabilization of the proton in a different water—requires an apparently much more rare event during which the pivot "plunges" into the aqueous phase (see episode at $t \sim 160$ ps). This has been observed in several independent proton-transfer episodes.

The overall consideration of the series of observations presented in the previous paragraphs seems to be sufficient to postulate a microscopic mechanism for proton translocations in micelles. The sequence would include the following two steps: (i) First, modifications in the connectivity pattern of the first solvation shell of the original pivot should be operated. These changes would involve the rupture of the HB shared between the potential new pivot water molecule and a surfactant oxygen site; (ii) in addition, the subsequent stabilization of proton in this new pivot would also require reestablishing a new HB with a third water molecule. Note that the latter step is facilitated by the migration of the charged complex toward the micelle core, where the number of potential water molecule candidates, acting as new HB acceptors, increases.

To provide additional arguments supporting the previous hypothesis, we finally examined the temporal behavior of two

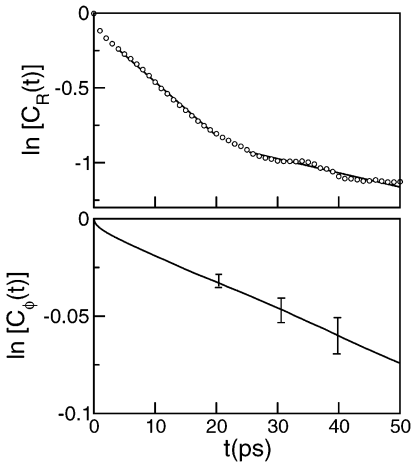

Figure 8. Time correlation functions for the relaxations of the pivot interfacial dynamics at the micelle surface. Top panel: distance to the center of mass of the micelle. Bottom panel: angular diffusion (see text).

relevant dynamical modes of the charged pivot within the micelle. More specifically, we examined the temporal relaxations of $R(t)$ and the one for cos $\phi(t)$, in terms of the following time correlation functions:

$$C_R(t) = \frac{\langle \delta R(t) \cdot \delta R(0) \rangle}{\langle (\delta R)^2 \rangle} \tag{12}$$

and

$$C_\phi(t) = \frac{\langle \delta \cos \phi(t) \cdot \delta \cos \phi(0) \rangle}{\langle (\delta \cos \phi)^2 \rangle} \tag{13}$$

The angular variable is defined as

$$\cos \phi(t) = \frac{\hat{\mathbf{z}} \cdot R(t)}{R(t)} \tag{14}$$

where $\hat{\mathbf{z}}$ represents a unit vector along an arbitrarily chosen direction of the local frame. Note that, because the excess proton remains mostly bound to the micelle boundary, cos $\phi(t)$ is the appropriate variable to describe the diffusive dynamics of the excess charge at the water/surfactant interface.

Results for the corresponding fluctuation relaxations for $R(t)$ and cos $\phi(t)$, are shown in Figure 8. After a brief transient, the decay of the $C_\phi(t)$ looks practically as single-exponential and is characterized by a very slow time scale in the nanosecond time domain. On the other hand, the long time behavior of the relaxation of fluctuations of $R(t)$ presents a biexponential decay,[55] with characteristic relaxation times $\tau_1 \sim 28$ ps and $\tau_2 \sim 105$ ps. We tend to believe that the shortest time scale might be directly associated with overall shape modifications of the interfacial cavity that hosts the excess proton. On the other hand, the similarities between the long time relaxations of $\delta R(t)$ and $\delta h(t)$ would confirm the relationship that might exist between proton transfers and the much more rare episodes during which a new HB is established with a third, inner water molecule.

V. Concluding Remarks

The computer simulation results presented in this paper shed light on several relevant aspects concerning the nature of protonic states in confined aqueous environments within reverse micelles. First, we have confirmed the propensity of the excess positive charge to exhibit interfacial solvation. This finding corroborates conclusions drawn from previous experimental studies, indicating pH gradients in the inner pools of reverse micelles and interfacial regions more acidic than the central nucleus.[8−13] Note that the interfacial solvation in reverse micelles can be interpreted in terms of simple entropic and energetic arguments. On one hand, the reversible work to bring the proton from the center to the interface of the micelle should necessarily include an ideal entropy term proportional to $-\ln(R)$. On the other hand, the observed interfacial solvation maintains intact the proton three-coordinated structure with its first solvation shell also observed in bulk; moreover, the dipolar alignment pointing toward the central part of the micelle is also energetically favorable, because it minimizes possible disruptions in the HB network of the aqueous phase. In this respect, the latter observation would bear many aspects in common with the anisotropy of the proton solvation structures previously observed at water−air interfaces,[56] water−Nafion membrane boundaries,[43] and bridging protons between hydrophobic and hydrophilic groups in water−methanol mixtures[41,48] as well.

More interestingly, our results also reveal that the stable solvation environments for protons in non-ionic reverse micelles differ at a qualitative level from those predicted by a recent Monte Carlo study of the solvation of simple cations in micelles. More specifically, Pal et al.[57] have analyzed the solvation of Li^+ in Na-AOT reverse micelles and found a tendency for core solvation. We tend to believe this feature reflects real, qualitative differences in the nature of the solvation of the two ionic species, a fact that is accordant with a unified molecular picture recently proposed to rationalize the singular behavior of adsorbed acids at water/air interfaces, compared with those exhibited by simple cationic species.[58]

The presence of water pockets in the interfacial region promotes proton trapping in local environments which present low HB connectivity with the rest of the aqueous phase. This affects the dynamics of HB and the nature of local polarization fluctuations, which, in turn, leads to a somewhat larger stabilization of Zundel-like structures. More importantly, the overall retardation affects the rate of proton transfer and the mechanisms that regulate jumps between neighboring water molecules. Our simulations show characteristic times for proton transfer τ_{tr}, which are intermediate between ∼100−150 ps; these values are to be compared with those observed in bulk water, which are on the order of 2−5 ps.

Given the similarities between the structures of the proton first solvation shells in bulk and micelle environments, the large difference observed between the τ_{tr} values suggests that transfer processes should be controlled by the HB dynamics in outer shells, most notably those involving water with hydroxyl and ether groups. Looking for clues to bring support to this line of reasoning, we analyzed the proton dynamics at the interface, focusing attention on pivot displacements along radial and angular coordinates. Fluctuations in the former displacements show two characteristic times: one relatively fast ($\tau_1 \sim$ 30 ps) and a second one, somewhat larger, on the order of $\tau_2 \sim$ 100 ps. Very likely, both timescales would correspond to dynamical modes promoting global changes in shape and roughness of the interface. Although we have not performed a rigorous trajectory analysis of proton-transfer events, a task that is well beyond the original scope of the present work, the similarity between the magnitudes of τ_2 and τ_{tr} leads us to conclude that the transfer dynamics is governed by modifications in the HB connectivity between the first and second solvation shells of the hydronium that would take place in inner regions of the micelles. Should this picture be confirmed by future

evidence, it will be also important to deeper analyze dynamical effects arising from disregarding diabatic states localized at hydroxyl and ether groups in the construction of $\hat{H}_{EVB}$.

Finally, we would like to comment on how the overall picture presented in this study might be affected by the absence of the nonpolar phase in our simulation experiments. As the proton solvation structures is concerned, we believe that this approximation should not pose any serious problem. This assertion is based on results from previous simulation studies, which show only minor changes operated in the water/surfactant interface when the nonpolar phase was explicitly incorporated.[24] On the other hand, from the dynamical side, it is very likely that we might not be capturing some remnant, long wavelength, dynamical modes originated in the nonpolar phase, affecting overall shape fluctuations of the micelle interface. In any event, the magnitude of these effects should remain necessarily small, because the weak coupling that prevails between the nonpolar phase modes and those of the micelle boundary is established along a rather thick surfactant shell of ~15 Å. As such, we anticipate that the modifications of the observed values of τ_2 and τ_{tr} should still be of order unity, and consequently, the dynamical conclusions concerning the disparities between the magnitudes of the proton-transfer rates in bulk and in micellar environments should remain physically sound.

Acknowledgment. J.R. and D.L. are staff members of CONICET-Argentina. The authors gratefully acknowledge financial support from the Direcció General de Recerca de la Generalitat de Catalunya (Grant 2005SGR00779) and the Ministerio de Educación y Ciencia of Spain (Grant BFM2003-08211-C03-01). FEDER funds from European Union (ref UNPC-E015) are also acknowledged.

References and Notes

(1) Jones, M. N.; Chapman, D. *Micelles, Monolayers, and Biomembranes*; John Wiley: New York, 1995.

(2) Luisi, P. K.; Straub, B. E. *Reverse Micelles: Biological and Technological Relevance of Amphiphilic Structures in Apolar Media*; Plenum Press: New York, 1984.

(3) *Structure and Reactiviy in Reverse Micelles*; Pileni, M. P. Ed.; Elsevier: Amsterdam, 1989.

(4) Bhattacharyya, K. *Acc. Chem. Res.* **2003**, *36*, 95.

(5) Nandi, N.; Bhattacharrya, K.; Bagchi, B. *Chem. Rev.* **2000**, *100*, 2013.

(6) More refined descriptions take the number of water states up to three, making a distinction between trapped, bound-next-to-surfactant, and free water. See, for example, ref 14.

(7) MacDonald, H.; Bedwell, B.; Gulari, E. *Langmuir* **1986**, *2*, 704. D'Arpano, A.; Lizzio, A.; Turco Liveri, V.; Alliota, F.; Vasi, C.; Migliardo, P. *J. Phys. Chem.* **1988**, *92*, 4436. Llor, A.; Rigny, P. *J. Am. Chem. Soc.* **1986**, *108*, 7533. De Marco, A.; Menegatti, E.; Luisi, P. L. *J. Biochem. Biophys. Methods* **1986**, *12*, 325. Hauser, H.; Haering, G.; Pande, A., Luisi, P. L. *J. Phys. Chem.* **1989**, *93*, 7869.

(8) Hasegawa, M. *Langmuir* **2001**, *17*, 1426.

(9) Holmes, J. D.; Ziegler, K. J.; Audriani, M.; Lee, C. T., Jr.; Bhargava, P. A.; Steytler, D. C.; Johnston, K. P. *J. Phys. Chem. B* **1999**, *103*, 5703.

(10) Baruah, B.; Roden, J. M.; Sedgwick, M.; Correa, M. N.; Crans, D. C.; Levinger, N. E. *J. Am. Chem. Soc.* **2006**, *128*, 12758.

(11) Bardez, E.; Goguillon, B.-T.; Jeh, E.; Valeur, B. *J. Phys. Chem.* **1984**, *88*, 1909. Bardez, E.; Monnier, E.; Valeur, B. *J. Phys. Chem.* **1985**, *89*, 5031.

(12) Politi, M. J.; Brandt, O.; Fendler, H. J. *J. Phys. Chem.* **1985**, *89*, 2345. Politi, M. J.; Chaimovich, J. *J. Phys. Chem.* **1986**, *90*, 282.

(13) Cohen, N.; Huppert, D.; Solntsev, K. M.; Tsfadia, Y.; Nachiel, E.; Gutman, M. *J. Am. Chem. Soc.* **2002**, *124*, 7539.

(14) Faeder, J.; Ladanyi, B. *J. Phys. Chem. B* **2000**, *104*, 1033.

(15) Faeder, J.; Ladanyi, B. *J. Phys. Chem. B* **2001**, *105*, 11148.

(16) Faeder, J.; Ladanyi, B. *J. Phys. Chem. B* **2005**, *109*, 6732.

(17) Laria, D.; Kapral, R. *J. Chem. Phys.* **2002**, *117*, 7712.

(18) Tobias, D. M.; Klein, M. L. *J. Phys. Chem.* **1996**, *100*, 6637.

(19) Senapati, S.; Berkowitz, M. L. *J. Phys. Chem. B* **2003**, *107*, 12906.

(20) Senapati, S.; Berkowitz, M. L. *J. Chem. Phys.* **2003**, *118*, 1937.

(21) Salaniwal, S.; Cui, S. T.; Cummings, P. T.; Cochran, H. D. *Langmuir* **1999**, *15*, 5188.

(22) Abel, S.; Sterpone, F.; Bandyopadhyay, S.; Marchi, M. *J. Phys. Chem. B* **2004**, *108*, 19458.

(23) Abel, S.; Waks, M.; Marchi, M.; Urbach, W. *Langmuir* **2006**, *22*, 9112.

(24) Allen, R.; Bondyopadhyay, S.; Klein, M. L. *Langmuir* **2000**, *16*, 10547.

(25) Warshel, A. *Computer Modeling of Chemical Reactions in Enzymes and Solutions*; Wiley: New York, **1980**. Aqvist, J.; Warshel, A. *Chem. Rev.* **1993**, *93*, 2523.

(26) For recent applications of MS-EVB schemes for protons in aqueous and biomolecular systems, see Voth, G. A. *Acc. Chem. Res.* **2006**, *39*, 143.

(27) Lobaugh, J.; Voth, G. A. *J. Chem. Phys.* **1996**, *104*, 2056.

(28) Schmitt, U. W.; Voth, G. A. *J. Chem. Phys. B* **1998**, *102*, 5547.

(29) Schmitt, U. W.; Voth, G. A. *J. Chem. Phys.* **1999**, *111*, 9361.

(30) Day, T. J. F.; Schmitt, U. W.; Voth, G. A. *J. Am. Chem. Soc.* **2000**, *122*, 12027.

(31) Day, T. J. F.; Soudackov, A. V.; Cuma, M.; Schmitt, U. W.; Voth, G. A. *J. Chem. Phys.* **2002**, *117*, 5839.

(32) Vuilleumier, R.; Borgis, D. *J. Phys. B* **1998**, *102*, 4261.

(33) Vuilleumier, R.; Borgis, D. *Chem. Phys. Lett.* **1998**, *284*, 71.

(34) Vuilleumier, R.; Borgis, D. In *Classical and Quantum Dynamics in Condensed Phase Simulations*; Berne, B. J., Ciccotti, G., Coker, D. F., Eds.; World Scientific: Singapore, 1998; Chapter 30.

(35) Vuilleumier, R.; Borgis, D. *J. Chem. Phys.* **1999**, *111*, 4251.

(36) Sagnella, D. E.; Tuckerman, M. E. *J. Chem. Phys.* **1998**, *108*, 2073.

(37) Brancato, G.; Tuckerman, M. E. *J. Chem. Phys.* **2005**, *122*, 224507.

(38) Kornyshev, A. A.; Kuznetsov, A. M.; Spohr, E.; Ulstrup, J. *J. Phys. Chem. B* **2003**, *107*, 3351.

(39) Walbran, S.; Kornyshev, A. A. *J. Chem. Phys.* **2001**, *114*, 10039.

(40) Laria, D.; Martí, J.; Guardia, E. *J. Am. Chem. Soc.* **2004**, *126*, 2125.

(41) Petersen, M. K.; Voth, G. A. *J. Phys. Chem. B* **2006**, *110*, 7085.

(42) Spohr, E.; Commer, P.; Kornyshev, A. A. *J. Phys. Chem. B* **2002**, *106*, 10560.

(43) Petersen, M. K.; Wang, F.; Blake, N. P.; Metiu, H.; Voth, G. A. *J. Phys. Chem. B* **2005**, *109*, 3727. Petersen, M. K.; Voth, G. A. *J. Phys. Chem. B* **2006**, *110*, 18594.

(44) Tepper, H. L.; Voth, G. A. *J. Phys. Chem. B* **2006**, *110*, 21327.

(45) Dang, L. X.; Pettit, B. M. *J. Chem. Phys.* **1987**, *91*, 3349.

(46) Berendsen, H. J. C.; van der Spoel, D.; van Drunen, R. *Comput. Phys. Comm.* **1995**, *91*, 43. Lindahl, E.; Hess, B.; van der Spoel, D. *J. Mol. Modell.* **2001**, *7*, 306. Schuettelkope, A. W.; van Aalten, D. M. F. *Acta Crystallogr.* **2004**, *D60*, 1355.

(47) Guss, L. S.; Kolthoff, I. M. *J. Am. Chem. Soc.* **1940**, *62*, 1494. Fillingim, T. G.; Luo, N.; Lee, J.; Robinson, G. W. *J. Phys. Chem.* **1990**, *94*, 6368. De Lisi, R.; Goffredi, M. *Electrochim. Acta* **1971**, *16*, 2181.

(48) Morrone, J. A.; Haslinger, K. E.; Tuckerman, M. E. *J. Phys. Chem. B* **2006**, *110*, 3712.

(49) Zundel, G.; Metzger, H. *Z. Phys. Chem.* **1968**, *244*, 456.

(50) Eigen, M.; de Maeyer, L. *Proc. R. Soc.* (*London*) **1958**, *A247*, 505.

(51) A slightly different, although equivalent, estimate was provided in ref 40.

(52) Chandler, D. In *Introduction to Modern Statistical Mechanics*; Oxford University Press: New York, 1987; Chapter 8.

(53) See, for example, Hadas, L.; Agmon, N.; Pettersen, M. K., Voth, G. A. *J. Chem. Phys.* **2005**, *122*, 14506, and references therein.

(54) This connectivity pattern has been found in micelles (see ref 24) and also in lamellar phases of $H_2O-C_{12}E_2$; see Bandyopadhyay, S.; Tarek, M.; Lynch, M. L.; Klein, M. L. *Langmuir* **2000**, *16*, 942.

(55) In fact, the correlation also presents also a short-time transient, which is not related with the proton-transfer process.

(56) Petersen, M. K.; Srinivasan, S. I.; Day, T. J. F.; Voth, G. A. *J. Phys. Chem. B* **2004**, *108*, 14804.

(57) Pal, S.; Vishal, G.; Gandhi, K. S.; Ayappa, K. G. *Langmuir* **2005**, *21*, 767.

(58) Mucha, M.; Frigato, T.; Levering, L. M.; Allen, H. C.; Tobias, D. J.; Dang, L. X.; Jungwirth, P. *J. Phys. Chem. B* **2005**, *109*, 7617.